Journal of Materials Chemistry C

Accepted Manuscript

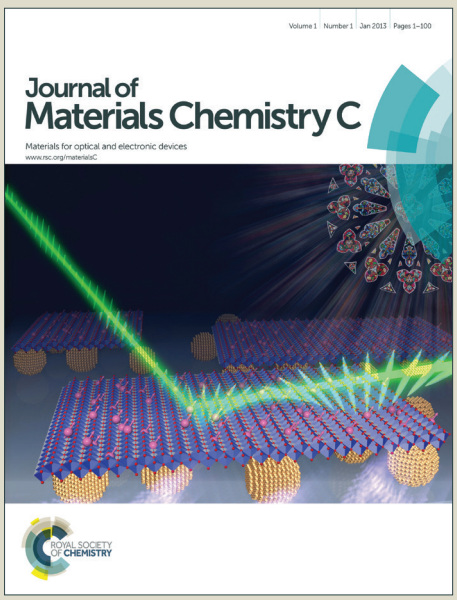

ROYAL SOCIETY OF CHEMISTRY

www.rsc.org/materialsC

Journal of
Materials Chemistry C

RSCPublishing

ARTICLE

Emission Red Shift and Energy Transfer Behavior of Color-tunable $KMg_4(PO_4)_3$:Eu^{2+}, Mn^{2+} Phosphors

Cite this: DOI: 10.1039/x0xx00000x

Jian Chen, Yan-gai Liu*, Lefu Mei, Ziyao Wang, Minghao Fang and Zhaohui Huang

Received 00th January 2012,
Accepted 00th January 2012

DOI: 10.1039/x0xx00000x

www.rsc.org/

Eu^{2+} and Mn^{2+} -co-doped $KMg_4(PO_4)_3$ phosphor was prepared via the conventional high temperature solid-state reaction. Their crystal structure, luminescence properties, emission red shift and energy transfer between Eu^{2+} and Mn^{2+} were investigated systematically. Under the excitation at 365 nm, $KMg_4(PO_4)_3$:Eu^{2+}, Mn^{2+} phosphors exhibited a broad excitation band ranging from 250 to 425 nm and two broad emission bands peaked at 450 nm and 625 nm which were ascribed from the 4*f*–5*d* transition of Eu^{2+} and the $^4T_1 \rightarrow {}^6A_1$ transition of Mn^{2+} ions, respectively. Three emission bands of Mn^{2+} were observed in $KMg_4(PO_4)_3$: Eu^{2+}, Mn^{2+}, which can be attribute to the disordering of the Mn^{2+} in Mg^{2+} sites to form the different luminescence centers. The energy transfer between the Eu^{2+} and Mn^{2+} ions is of a resonant type via a dipole–quadrupole mechanism. The emission red shift with increasing Mn^{2+} concentration and operating temperature are discussed in relation with crystal structure and energy transfer in $KMg_4(PO_4)_3$:Eu^{2+}, Mn^{2+}. Utilizing the redshift and the energy transfer from Eu^{2+} to Mn^{2+}, $KMg_4(PO_4)_3$:Eu^{2+}, Mn^{2+} phosphor can be tuned from blue to pink by appropriate adjusting the Mn^{2+} content and may have potential application for white light-emitting diodes and plantlets cultured.

1 Introduction

Along with the expanding market, the phosphor-converted light-emitting diodes (pc-LEDs), which were restricted to niche applications (flashlights and traffic lights), are now developing their way into general lighting applications and plantlets cultured.[1-6] Currently, the research of color tuning of phosphors has received great attention owe to its potential application in improved white LEDs and plant growth.[2,3] The most prevalent white light LEDs in market are assembled by combination of blue InGaN chip and the yellow-emitting YAG/Ce phosphor.[4] However, due to the lack of the red region, this white LED shows a relatively cool white light, hence, it is significant to develop the single host emission color-tunable phosphor with near-ultraviolet (n-UV) chip LED to integrate the white pc-LEDs with excellent Color Rendering Index (CRI) and appropriate Correlated Color Temperature (CCT).[5]

Moreover, considerable interest has been paid in the use of LEDs as a radiation source for plantlets cultured in recent years due to their vast potential for commercial application.[3] The plantlets cultured rely on photosynthesis which is a process in green plants or other organisms. This process can convert light energy from the sun into chemical energy that can supply the organisms' activities.[6] However, chlorophylls, the organ used for photosynthesis, mainly absorb red (600-700 nm) and blue (430-480 nm) lights during the process of photosynthesis. Hence, red and blue emitting LEDs can improve the photosynthesis of plant, and then reduce the growth time and boost the yield.[7,8] Owing to small in size, long lifetime, solid state construction and wavelength specificities, LEDs have been applied in many areas of photobiological research such as morphogenesis[9], algal photo bioreactor[10], photosynthesis[11] as well as chlorophyll synthesis[12] and several plant species have been grown successfully under LEDs, including seedlings of lettuce, pepper, cucumber, wheat, spinach[7-14]. However, various plants need different red region; therefore, a blue-red phosphor with red-shifted emission to adjust the red region for adapting various plants is imperative to develop.[4-15]

The Eu/Mn-coactivated is an available strategy to generate the blue and red emitting light in phosphor at same time under

n-UV excitation. The Mn^{2+} ions doped phosphor presents a broad band emission derived from the $^4T_1 \rightarrow {}^6A_1$ transition. Owing to within in the 3d shell, the electrons of the Mn^{2+} ion are strongly coupled to lattice vibration and influenced by site symmetry and crystal field strength of host.[16,17] Thus, The emission of Mn^{2+} can be tuned from green (strong crystal field) to red (weak crystal field) via adjusting the site symmetry and crystal field strength of host. However, due to the forbidden d–d transitions of Mn^{2+}, the absorption and emission of Mn^{2+} are weak. Therefore, the Eu^{2+} is usual to sensitize Mn^{2+} in numerous hosts.[18–21]

Orthophosphate crystals attract considerable attention as luminescence hosts due to advantages of easy preparation, cheap raw materials, good chemical stability, and satisfactory absorption in the n- UV region. Tomaszewski and co-workers first acquired the orthophosphate compound $KMg_4(PO_4)_3$ crystal from flux during crystallizing $K_2MgWO_2(PO_4)_2$.[12] They investigated the crystal structure and vibrational properties of $KMg_4(PO_4)_3$. In this type of phosphors, various dopant ions can be introduced, because two kinds of cations (alkali and alkaline earth cations) have ionic radii large enough for substitution. Lan et al. reported the luminescence properties of Eu^{2+}-activated $KMg_4(PO_4)_3$ by combustion-assisted synthesis method in 2012.[13] In addition, three types coordination environment of magnesium were discovered and the ion radius of Mg^{2+} is similar to Mn^{2+}, indicating the emission shift of Mg^{2+} will be expected.

In the present work, Eu^{2+} and Mn^{2+} -co activated $KMg_4(PO_4)_3$ phosphors were prepared by the conventional high temperature solid-state reaction. Their luminescence properties and energy transfer between Eu^{2+} and Mn^{2+} were investigated, respectively. The wavelength position of emission red shift, full wavelength at half-maximum (FWHM), temperature-dependent emission spectra, and color coordinates were investigated and the related mechanisms were discussed in detail.

2 Experimental

2.1 Materials and Syntheses

Eu^{2+} or Mn^{2+} singly doped samples $KMg_4(PO_4)_3$: Eu^{2+}, $KMg_4(PO_4)_3$: Mn^{2+}, and Eu^{2+}, Mn^{2+} co-doped $KMg_4(PO_4)_3$: Eu^{2+}, Mn^{2+} phosphors were all prepared through the traditional high temperature solid-state method. The starting materials were a stoichiometric mixture of KH_2PO_4 (A. R.), MgO (A. R.), $NH_4H_2PO_4$ (A. R.), $MnCO_3$ (A. R.) and Eu_2O_3 (A. R.) and ground homogeneously in agate mortar. The mixtures of these materials were firstly heated at 600°C for 2 h in a muffle furnace in air to release NH_3, CO_2, and H_2O. After that the precursor was reground and stinted at 1000°C for 6 h in a reducing atmosphere (H_2/N_2) in a tube furnace. Finally the furnace cooled to room temperature and the samples were ground in an agate mortar.

2.2 Characterization Method

X-ray powder diffraction (XRD) patterns of the final products were identified on a D8 Advance diffractometer (Bruker Corporation, Germany) with Cu Kα radiation (λ = 0.15406 nm) radiation. The photoluminescent excitation/emission (PLE/PL) spectra were detected by a Hitachi F-4600 fluorescence spectrophotometer (Japan) equipped using a 150 W Xe lamp as the excitation source. The temperature-dependent luminescence properties were measured on the same spectrophotometer which was assembled with a computer-controlled electric furnace and a self-made heating attachment. The room-temperature luminescence decay curves were obtained from a spectrofluorometer (Horiba, Jobin Yvon TBXPS) using a tunable pulse laser radiation (nano-LED) as the excitation. The quantum efficiency was detected by an integrating sphere in the FLS920 fluorescence spectrometer (Edinburgh Instruments) at room temperature. The luminous efficiency of the fabricated white LED was obtained using PMS-80 Sync-Skan color analyser system under a forward bias of 20 mA.

3 Results and Discussion

3.1 Crystal Structures and Phase Analysis

The orthophosphate $KMg_4(PO_4)_3$ crystallizes in a orthorhombic cell, with the space group Pnnm(No. 58). The crystal structure of $KMg_4(PO_4)_3$ and the coordination environment of the K and Mg atoms are present in Figure 1. The structure of $KMg_4(PO_4)_3$ consists of four types of polyhedra sharing common edges and corners which build a three-dimensional framework and form the tunnels along directed b-axis. The K^+ ions are located in the tunnels and 8-fold coordinated by oxygen atoms with 4g position and m site symmetry.[12] The four types of polyhedra respectively are one [PO_4] tetrahedron and three types of magnesium–oxygen polyhedral and can be distinguished in the structure. Two types of Mg^{2+} ions are 6-fold coordinated by oxygen atoms and the third type is 5-fold coordinated by oxygen atoms. Thus, there exist one K^+ sites and three different Mg sites (Mg (I), Mg (II), and Mg (III)), as shown in Figure 1. The average distances of K-O, Mg(I)-O, Mg(II)-O, and Mg(III)-O are 2.8943, 2.1403, 2.1212 and 2.0224 Å, respectively.

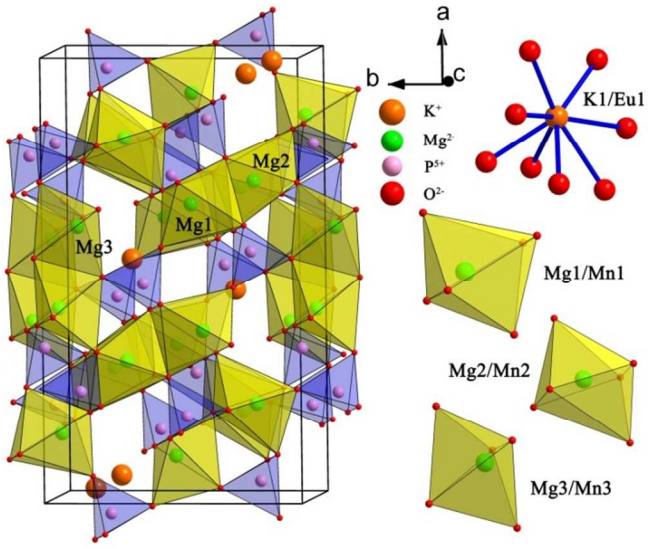

Fig. 1 Crystal structure of the $KMg_4(PO_4)_3$: Eu^{2+}, Mn^{2+} and the coordination environment of the cations (K and Mg).

The phase structures of the as-synthesized $KMg_4(PO_4)_3$: $0.04Eu^{2+}$, xMn^{2+} (x = 0, 0.04, 0.08, and 0.16) and $KMg_4(PO_4)_3$ host were characterized by XRD measurements and compared with standard pattern (JCPDS 15-4111) of $KMg_4(PO_4)_3$ in the Figure 2. All the XRD patterns match well with the standard pattern, and no second phase can be detected, indicating the formation of single phase of $KMg_4(PO_4)_3$: Eu^{2+}, Mn^{2+}. When Eu^{2+}, Mn^{2+} ions are incorporated into the crystal structures of $KMg_4(PO_4)_3$, Eu^{2+}, Mn^{2+} ions may substitute all the cationic sites of K^+ and Mg^{2+} (I, II, and III). As the Figure 2(b) shown, when the Eu^{2+} ions were doped into the $KMg_4(PO_4)_3$ host, the main diffraction peaks of (002) shifted slightly to the higher angle side. However, as the Mn^{2+} ions were doped and increased with concentration, the diffraction peaks gradually shifted to the lower angle side. This changes indicates that the Eu^{2+} ions substituted the comparatively big radius ions in $KMg_4(PO_4)_3$ host lattice and Mn^{2+} ions replaced the comparatively small radius ions. [14] Additionally, an acceptable percentage difference of the ion radii between the doped and substituted ions should not exceed 30%.[15] Hence, it is practicable to consider that Eu^{2+} (r = 1.25 Å for coordinate number (CN) = 8 and r = 1.17 Å for CN = 6) ions substituted the position of K^+ (r = 1. 51 Å for CN = 8) and Mn^{2+} (r = 0.83 Å for CN = 6 and r = 0.75 Å for CN = 5) ions replaced the location of Mg^{2+} (r = 0.72 Å for CN = 6 and r = 0. 66 Å when CN = 5). The sites of P^{5+} (r = 0. 17 Å for CN = 4) are too small to accept Eu^{2+} or Mn^{2+} ions.

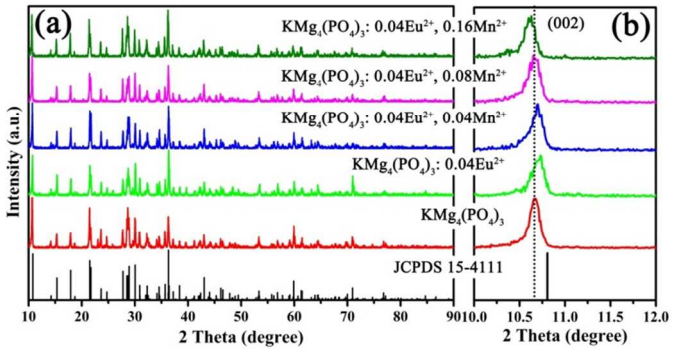

Fig. 2 XRD patterns of the as-prepared samples $KMg_4(PO_4)_3$: $0.04Eu^{2+}$, xMn^{2+} (x = 0, 0.04, 0.08, and 0.16), $KMg_4(PO_4)_3$ host and the standard pattern (JCPDS 15-4111) (a); the detailed XRD patterns ranging from 10° to 12° for the same samples (b).

3.2 Room-Temperature Photoluminescence Properties of $KMg_4(PO_4)_3$: Eu^{2+}, Mn^{2+}

The excitation and emission spectra of the $KMg_4(PO_4)_3$: $0.02Eu^{2+}$ phosphor are shown in Figure 3a. The excitation spectrum monitored at 450 nm shows broad excitation from 250 to 425 nm which derive from $4f$–$5d$ transition of Eu^{2+} ions. Three distinct excitation peaks at 300, 350 and 380 nm are observe, which may be due to the electronic transitions from the ground state to the different crystal field splitting bands of excited 5d states of Eu^{2+}.[16] Under 300 nm excitation, the phosphor gives a blue emission band peaked at 450 nm due to the $4f^6 5d$–$4f^7$ transitions of Eu^{2+}.

Figure 3b illustrated the excitation and emission spectra of $KMg_4(PO_4)_3$: $0.06Mn^{2+}$. The excitation spectrum includes several bands from 250 to 500 nm, peaking at 365, 410, 465 and 564 nm which originated to the ground state $^6A_1(^6S)$ to the excited states $^4T_2(^4D)$, [$^4A_1(^4G)$, $^4E(^4G)$], $^4T_1(^4G)$ and $^4T_2(^4G)$, respectively. Upon 410 nm excitation, the $KMg_4(PO_4)_3$: $0.06Mn^{2+}$ phosphor shows an asymmetric emission band ranging from 550 to 800 nm due to the spin-forbidden $^4T_1(4G) \rightarrow {}^6A_1(6S)$ transition of Mn^{2+} ions.[17,18] According to the three kinds of Mg^{2+} sites, the emission spectrum can be deconvoluted into three Gaussian components that peaked at 625, 681 and 719 nm, respectively. According to the Tanabe–Sugano diagrams, the emission spectrum of Mn^{2+} ions relies strongly on the crystal field strength of the host lattices.[19] The weak crystal field around Mn^{2+} ions will reduce the splitting of the excited 3d energy levels and generate higher energy Mn^{2+} emission. Oppositely, the Mn^{2+} ions will emit low energy light with the strong crystal field.[20,21] In $KMg_4(PO_4)_3$, The first type of the Mg(I)-octahedral is surrounded by PO_4 groups and exclusively connect as well as share one edge with it. In the second kind, the Mg(II)-octahedral shares edges with two neighbouring octahedra to form the chains oriented along c-axis and also shares one edge with a phosphate tetrahedron. The third type of Mg(III) is 5-fold co-ordination and two adjacent [MgO_5] polyhedron are edge-shared to form the [Mg_2O_8] bi-

polyhedron.[12] Owing to the strong bonding of PO_4-tetrahedron, we can conclude that the band peaked at 625 nm can be attributed to the transition of Mn^{2+} ions occupying the Mg(III) sites, the band peaked at 681 and 719 are due to the transition of Mn^{2+} ions occupying the Mg(II) and Mg(I) sites, respectively.

As seen in Figure 3a,b, a significant spectral overlap between the PL spectrum of $KMg_4(PO_4)_3$: $0.02Eu^{2+}$ phosphor and PLE spectrum of $KMg_4(PO_4)_3$: $0.06Mn^{2+}$ phosphor is obtain, which is a typical signal of resonance-type energy transfer between the sensitizer Eu^{2+} ions and activator Mn^{2+} ions. It can be further proved by the PLE spectra in Figure 3c. The PLE spectra of $KMg_4(PO_4)_3$:$0.02Eu^{2+}$,$0.6Mn^{2+}$ monitored by 620, 650, 680 and 700 nm (emissions of Mn^{2+}) is in consistent with that monitored by 450 nm (emission of Eu^{2+}) in addition to the difference of the relative intensity, demonstrating the happened of energy transfer from Eu^{2+} to Mn^{2+}. Besides, the PL spectrum of $KMg_4(PO_4)_3$: Eu^{2+}, Mn^{2+} phosphor excited by 365 nm presents not only blue-emitting light of Eu^{2+} ions, but also red-emitting light of the Mn^{2+} ions, indicating the color-tunable $KMg_4(PO_4)_3$:Eu^{2+}, Mn^{2+} phosphors were obtained.

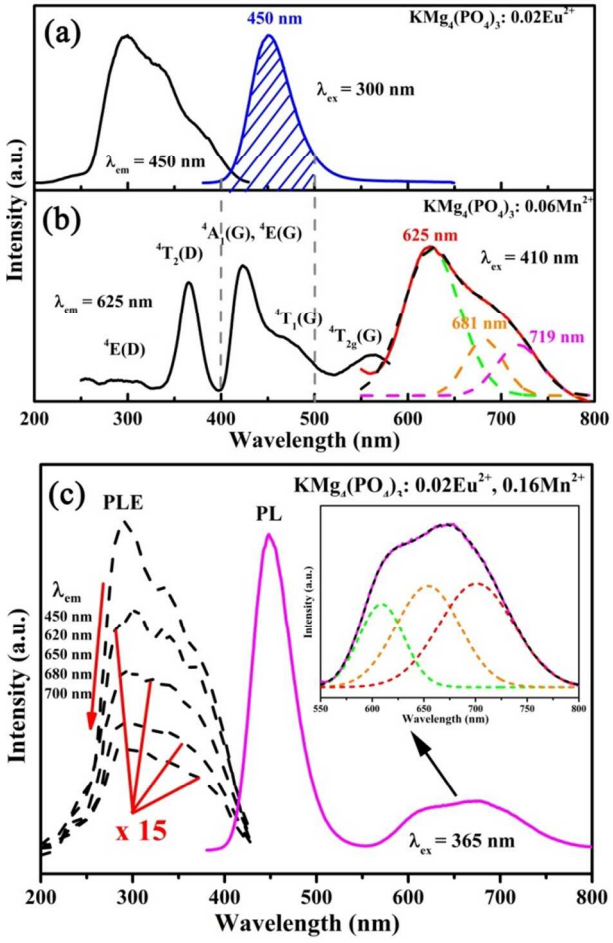

Fig. 3 Excitation and emission spectra of $KMg_4(PO_4)_3$: $0.02Eu^{2+}$ (a), $KMg_4(PO_4)_3$: $0.06Mn^{2+}$ (b) and $KMg_4(PO_4)_3$: $0.02Eu^{2+}$, $0.06Mn^{2+}$ (c). The corresponding monitoring wavelengths are given in the figure.

3.3 Energy Transfer Between Eu^{2+}-Mn^{2+} in $KMg_4(PO_4)_3$ Host

Figure 4 depicts the dependence of emission intensity by excitation at 365 nm on various Mn^{2+} doping concentrations in $KMg_4(PO_4)_3$:Eu^{2+}, xMn^{2+} (x = 0 – 0.35) phosphors. The emission intensity of the Eu^{2+} ions decreased as the Mn^{2+} doping concentration increasing, while the intensity of the Mn^{2+} ions increased. These changes of spectra can be attributed to the energy transfer from Eu^{2+} to Mn^{2+} ions. Moreover, an obviously red shift (620-690 nm) is observed on the peak wavelength of Mn^{2+} along with the increasing of Mn^{2+} concentration. This result will discuss in detail in Section 3.4.

The proposed diagram of the energy transfer process from Eu^{2+} to Mn^{2+} in $KMg_4(PO_4)_3$ phosphor is illustrated in Figure 5. From this diagram, the energy transfer behavior between Eu^{2+} and Mn^{2+} ions can be attributed to the similar value of energy level between the excited 5d state of Eu^{2+} and the $^4E(^4D)$ levels of Mn^{2+} ions.[22,23] To further demonstrate the energy transfer from Eu^{2+} to Mn^{2+} ions, the fluorescent decay curves of Eu^{2+} in different Mn^{2+} doping contents (0, 0.02, 0.04, 0.08, 0.12, 0.16), which are monitored at 450 nm and excited at 370 nm, are illustrated in Figure 6. The entire decay curves can be well fitted to a single-exponential decay model by the following equation: [21]

$$I(t) = A \exp(-t/\tau) \quad (1)$$

where I means the luminescence intensity; A is a constant; t is time; and τ means the lifetimes for the exponential components. As shown in Figure 5, the obtained lifetimes monitored at 450 nm decrease from 1264.93 to 530.94 nm, corresponding to x = 0-0.35. The decrease of the donor decay times indicates that non-radiative energy transfer works, because the donor decay times of radiative energy transfer will remain constant in the absence and presence of acceptor.[22] Additionally, the decay curves of $KMg_4(PO_4)_3$:$0.02Eu^{2+}$, xMn^{2+} phosphors monitored at 450 nm gradually got less linear with increasing Mn^{2+} concentration, which also is a typical sign of energy transfer.[23,24]

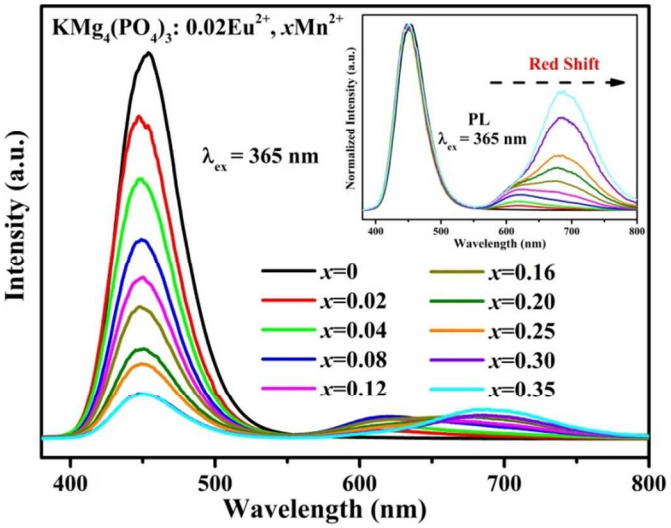

Fig. 4 The emission spectra of $KMg_4(PO_4)_3$: $0.02Eu^{2+}$, xMn^{2+} (x = 0 – 0.35) phosphors. (inset) The normalized emission spectra for $KMg_4(PO_4)_3$: $0.02Eu^{2+}$, xMn^{2+} (x = 0 – 0.35) phosphors.

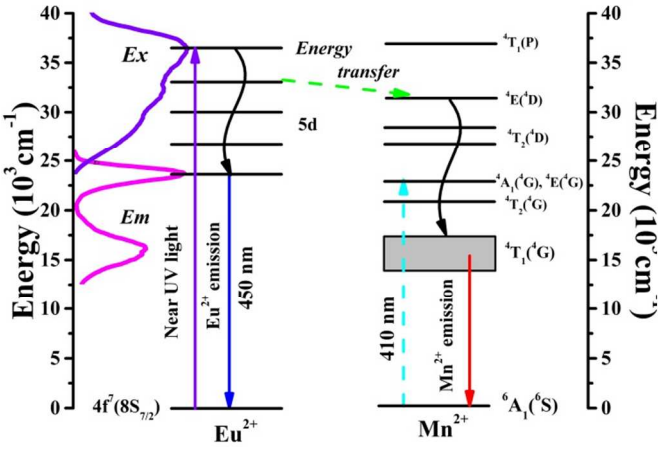

Fig. 5 Schematic diagram of energy transfer in $KMg_4(PO_4)_3$: Eu^{2+}, Mn^{2+}.

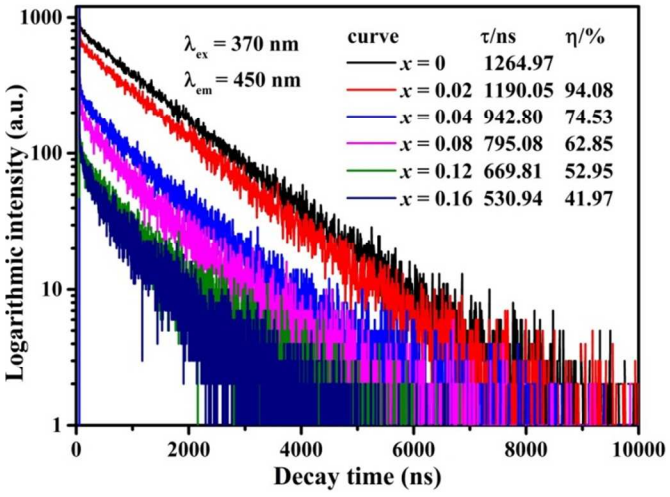

Fig. 6 Decay lifetime tests of $KMg_4(PO_4)_3$: $0.02Eu^{2+}$, xMn^{2+} (x = 0 – 0.16) detected at 450 nm for Eu^{2+} emission.

The efficiency of energy transfer from Eu^{2+} to Mn^{2+} can be estimated according to the following equation:

$$\eta = 1-\tau_s/\tau_{s0} \quad (2)$$

where η means the energy transfer efficiency; τ_s and τ_{s0} are on behalf of the lifetimes of Eu^{2+} in the absence and the presence of Mn^{2+}, respectively. As given from the inset of Figure 6, the efficiency of energy transfer ascends gradually with the increment of the concentration of Mn^{2+}.

In general, the energy transfer mechanism from Eu^{2+} to the Mn^{2+} ions via electric multipolar interaction and the relation can be adopted by the Dexter's energy transfer formula:[25,26]

$$\frac{I_{S0}}{I_S} \propto C^{n/3} \quad (3)$$

in which Is_0 and Is stand for the luminescence intensities of Eu^{2+} with and without activator Mn^{2+} present, respectively; C means the dopant concentration of Mn^{2+}; and n = 6, 8, and 10 correspond to dipole-dipole, dipole-quadrupole, and quadrupole-quadrupole interactions, respectively. The relationships between (I_{S0}/I_S) versus $C^{n/3}$ are shown on Figure 7a-7c, which reveal a linear behavior only when n = 8, indicating that the energy transfer mechanism from Eu^{2+} to Mn^{2+} in the $KMg_4(PO_4)_3$ host follows a nonradiative electric dipole-quadrupole interaction.

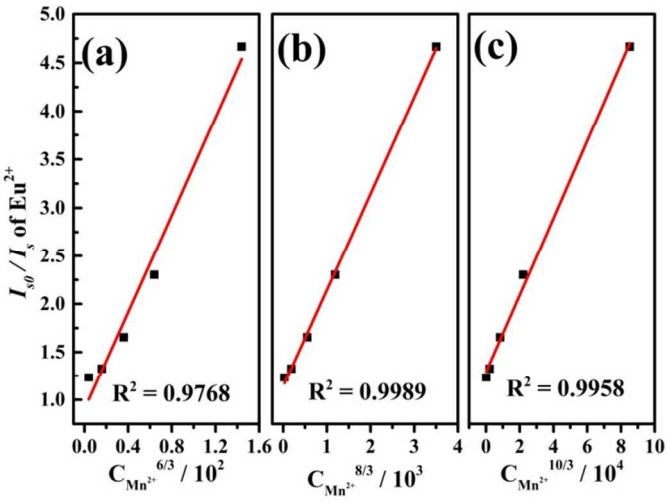

Fig. 7 Dependence of I_{s0}/I_s of Eu^{2+} on $C_{Mn2+}^{6/3}$ (a), $C_{Mn2+}^{8/3}$ (b), $C_{Mn2+}^{10/3}$ (c).

3.4 The Red Shift of Concentration- and Temperature-Dependent Emission Spectra

As given in Figure 8, a continuous redshift is observed on the peak wavelength of Mn^{2+} along with the increasing of Mn^{2+} concentration. There are two aspects can be explained this

phenomenon. On the one hand, since the ion radius of Mn^{2+} is larger than Mg^{2+}, the Mn–O distances would shorten with an increase in Mn^{2+} doping, and then cause in the stronger crystal field.[19] Therefore, the crystal would experience a compressive stress and the 3d energy levels of Mn^{2+} ions may experience an influence from the nearest neighbor oxygen, leading to emission red shift.

On the other hand, the probability of the energy transfer between the Mn^{2+} ions is increased via decreasing the average distance between the ions, when the concentration of Mn^{2+} increases. The main mechanism of energy transfer can be include in two types: exchange interaction or electric multipolar interaction.[27] For further research the process of energy transfer between the Mn^{2+} ions, the critical distance for energy transfer can be reckoned via the following equation:[28]

$$R_c \approx 2\left(\frac{3V}{4\pi x_c N}\right)^{\frac{1}{3}} \quad (4)$$

in which V means the unit cell volume (965.361 $Å^3$), x_c represents the concentration of activator ion where the quenching occurs (0.08) and N is the number of the Mg^{2+} ion in per unit cell (12). Hence, the value of R_c is calculated to about 12.43 Å. Since the typical critical distance of the exchange interaction is about 5 Å, therefore, the electric multipolar interactions are dominant in the energy transfer process.[29,30] The electric multipolar interactions transfer is nonradiative and would lead to the excited 5d electron transfer to a relatively lower energy level (redshift). Thus, a redshift emission is observed with increasing Mn^{2+} concentration.

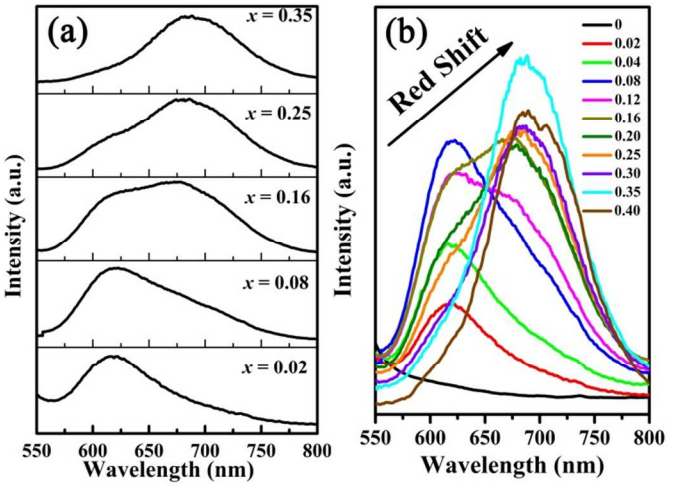

Fig. 8 The normalized emission spectra of $KMg_4(PO_4)_3$: $0.02Eu^{2+}$, xMn^{2+} (x = 0.02, 0.08, 0.16, 0.25, 0.35) (a) and the emission spectra of $KMg_4(PO_4)_3$: $0.02Eu^{2+}$, xMn^{2+} (x = 0 – 0.40) (b) from 550 nm to 800 nm.

The FWHM values and peak position of the Mn^{2+} ions emission peak band in $KMg_4(PO_4)_3$ are shown in Figure 8. Along with the increase of Mn^{2+} concentration, the FWHM values of the emission gradually becomes larger, whereas it reduces as x = 0.16. It is easy to explain that the larger emission FWHM is due to the enhanced disordering of the Mn^{2+} in Mg^{2+} sites with the increase in Mn^{2+} concentration.[19] The reduction of the emission FWHM is caused by the energy transfer between Mn^{2+} ions and the increase in crystal field.[31] As mentioned above, There are three nonequivalent Mn^{2+} sites in $KMg_4(PO_4)_3$ lattice. When the lower concentration of Mn^{2+} doped in $KMg_4(PO_4)_3$, the average distance between the luminescence center of Mn^{2+} in the lattices was long enough to neglect the energy transfer between the nonequivalent Mn^{2+}. Along with the increase of Mn^{2+} doping, the probability of the energy transfer from the Mn^{2+} ions in the higher energy level sites to that in lower energy level sites gradually increased. Hence, the overlapping of the different luminescence centers became weak, resulting in the smaller FWHM values of the Mn^{2+} emission. Additionally, as presented in Figure 9, the symmetry of emission spectra become low with the increase of Mn^{2+} concentration, and then heighten as x = 0.16. The variation tendency of the symmetry of emission spectra is in coordination with that of the FWHM values of the emission and corresponds to the above analysis.

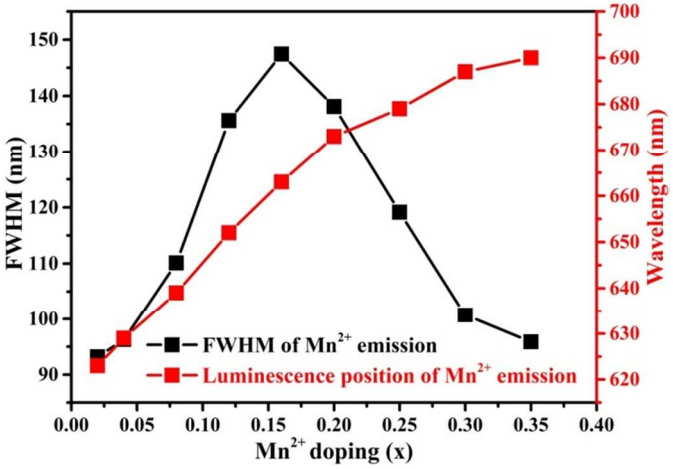

Fig. 9 The FWHM and peak position of the Mn^{2+} ions emission peak band in $KMg_4(PO_4)_3$: $0.02Eu^{2+}$, xMn^{2+} (x = 0 – 0.35).

Figure 10 depicts the temperature-dependent emission spectra of $KMg_4(PO_4)_3$: $0.02Eu^{2+}$, $0.35Mn^{2+}$. As shown in the inside of Figure 9, the PL intensities of the characteristic peaks of Eu^{2+} and Mn^{2+} only decay by 12.77% and 19.52% of the initial intensities at room temperature. The results demonstrate that the as-prepared $KMg_4(PO_4)_3$: $0.02Eu^{2+}$, $0.35Mn^{2+}$ phosphor exhibits a high temperature quenching. The interaction of electron–phonon in both the ground state and excited state of luminescence center are responsible for the emission intensities decreased with temperature increment. This nonradiative transition probability rely on temperature which bring about the decrease in emission intensity.[32] Besides, the interaction of electron–phonon in both the ground state and excited state will also cause the emission peaks shift to a lower energy, which can be explained by the Varshni equation:[33]

$$E(T) = E_0 - \frac{aT^2}{T+b} \quad (5)$$

in which E(T) means the energy difference between excited states and ground states at a temperature T, E_0 presents the energy difference at 0 K, and a and b are fitting parameters. Nevertheless, a distinct blue shift of the emission peaks with increasing temperature is observed in Figure 9. It may attribute to the thermally activated phonon-assisted tunneling from the excited states of the low energy emission band to that of the high energy emission band, which can be illustrated from the configuration coordinate diagram.[34] In $KMg_4(PO_4)_3$: Eu^{2+}, Mn^{2+}, there are at least three luminescence centers for Mn^{2+} ions. At a low temperature, the barrier of high energy emissions [Mn[II]] and [Mn[III]] are hard to overcome, and the low energy emission Mn[I] is dominant. When the temperature increases, the thermal back-transfer is gradual over the barrier of high energy emissions [Mn[II]] and [Mn[III]], and consequently the higher energy emission [Mn[II]] and/or [Mn[III]] are dominant gradually. Therefore, a blueshift behavior with increasing temperature is observed.

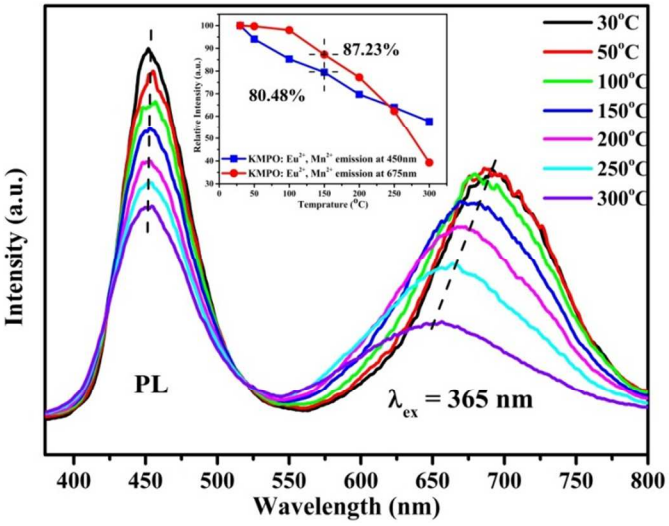

Fig. 10 Temperature-dependent PL spectra of $KMg_4(PO_4)_3$: $0.02Eu^{2+}$, $0.35Mn^{2+}$. The inset shows the emission intensity versus temperature.

Figure 11 illustrates the variation of Commission International del' Eclairange (CIE) chromaticity coordination of the $KMg_4(PO_4)_3$: $0.02Eu^{2+}$, xMn^{2+} (x = 0, 0.04, 0.08, 0.16, 0.25, 0.35) phosphors excited at 365 nm. The color of these phosphors can be modulated from blue (0.1479, 0.0663) to pink (0.2683, 0.1496) with the increasing concentration of the Mn^{2+} ions. The homologous digital photographs of the selected $KMg_4(PO_4)_3$: $0.02Eu^{2+}$, xMn^{2+} phosphors under a 365 nm UV lamp irradiation are depict in the inset of Figure 9. It is believed that the series of $KMg_4(PO_4)_3$: $0.02Eu^{2+}$, xMn^{2+} phosphors exhibit promising potential as phosphor candidates used for white LEDs or plant growth.

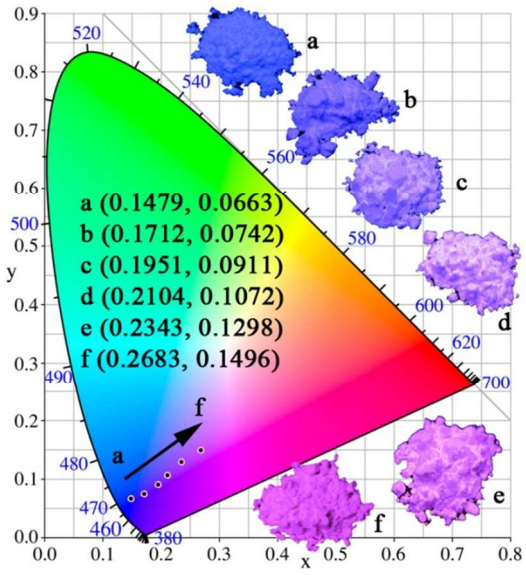

Fig. 11 CIE chromaticity coordinates of $KMg_4(PO_4)_3$: $0.02Eu^{2+}$, xMn^{2+} (a) x = 0; (b) x = 0.04; (c) x = 0.08; (d) x = 0.16; (e) x = 0.25; (f) x = 0.35) phosphors under 365 nm excitation and the corresponding samples digital images excited at 365 nm in UV box.

3.5 Potential application in plantlets cultured and white light-emitting diodes.

The quantum yield (QY) is an important parameter for the practical application of phosphors. The QYs of $KMg_4(PO_4)_3$:$0.04Eu^{2+}$, xMn^{2+} (x = 0.02, 0.08, 0.20, 0.35) were measured under 330 nm excitation. Accordingly, the PL QYs of blue emission (380-550) were estimated as 95%, 60%, 22% and 10% as well as red emission (550-800) were calculated as 22%, 58%, 73% and 73%, respectively. The standard terrestrial (AM1.5) solar irradiation spectrum covers ultra-broad wavelength region from ultraviolet to infrared and absorption spectra of chlorophylls are shown in Figure 12a. It can be observed that the lights used by green plants for photosynthesis are only a very small part in the whole solar spectra. Thus, the double emitting (blue and red) $KMg_4(PO_4)_3$:Eu^{2+}, Mn^{2+} phosphors may find potential application in photosynthesis of green plants by improving the photosynthesis of plant at day and night, which will reduce the growth time and boost the yield of plants.

To assess the potential application of $KMg_4(PO_4)_3$:Eu^{2+}, Mn^{2+} phosphor for white LEDs, the electroluminescence spectra of white LED lamps fabricated using a n-UV 385 nm chip combined with $KMg_4(PO_4)_3$:$0.04Eu^{2+}$, $0.35Mn^{2+}$ phosphor and green-emitting $(Ba,Sr)_2SiO_4$:Eu^{2+} phosphor driven by forward bias current of 30 mA and image of LED lamp package was measured as presented in Figure 12b. The electroluminescent spectrum obviously shows four emission bands at 385, 550, 450 and 680 nm, which are ascribed to the 385-nm NUV chip, $(Ba,Sr)_2SiO_4$:Eu^{2+} emission, Eu^{2+} emission and Mn^{2+} emission of $KMg_4(PO_4)_3$, respectively. The CIE color coordinates,

correlated color temperature (CCT) and color rendering index (Ra) of this fabricated white LED lamp are respectively detected to be (0.27, 0.32), 9882.63 and 84.99, indicating that the $KMg_4(PO_4)_3$:Eu^{2+}, Mn^{2+} may be a promising phosphor for application of white LEDs. The luminous efficiency of the fabricated white LEDs is ~5.757 lm/W, which is lower than commercial white LEDs because of the rough fabrication process and poor chip efficiency. Thus, the efficiency can be further enhanced by optimizing the luminescence properties of the phosphors, the fabrication process of the white LEDs and improving the chip efficiency.[21,47]

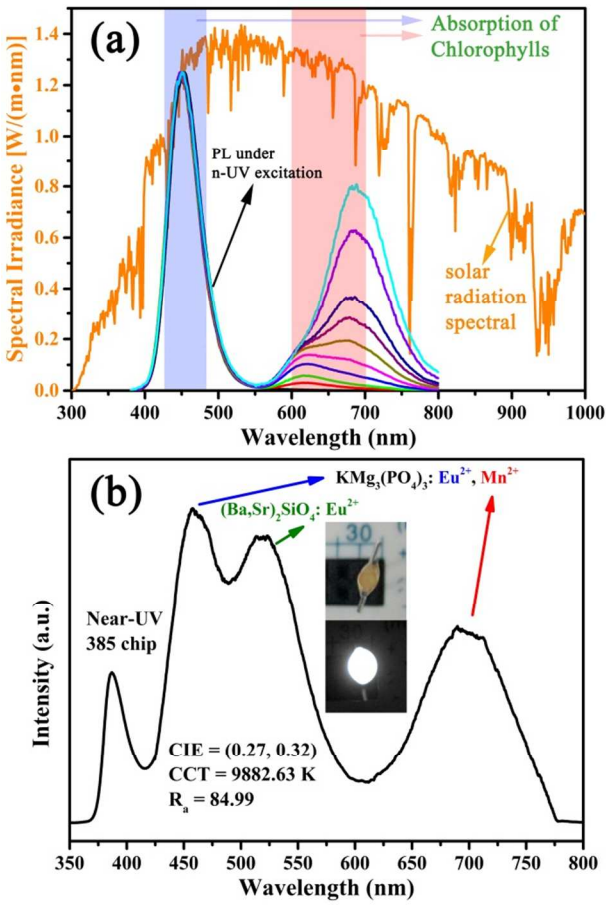

Fig. 12 (a) The standard terrestrial (AM1.5) solar irradiation spectrum, absorption spectra of chlorophylls and the PL spectra of $KMg_4(PO_4)_3$: Eu^{2+}, Mn^{2+} phosphors under n-UV excitation; (b) Electroluminescence spectra of *w*-LED lamp fabricated via the combination of a NUV 385-nm chip, green-emitting $(Ba,Sr)_2SiO_4$:Eu^{2+} phosphor and $KMg_4(PO_4)_3$:0.04Eu^{2+}, 0.35Mn^{2+} phosphor. Inset shows digital images of the LED package with and without powder input.

4 Conclusions

A series of Eu^{2+} and Mn^{2+} -co activated $KMg_4(PO_4)_3$ phosphor was prepared by the conventional high temperature solid-state reaction. The substitution sites of Mn^{2+} were proved for Mg^{2+} sites and three types of substitution sites are identified for Mn^{2+} in $KMg_4(PO_4)_3$ lattice. Their luminescence properties and energy transfer between Eu^{2+} and Mn^{2+} were investigated systematically. Three emission bands of Mn^{2+} were observed in $KMg_4(PO_4)_3$: Eu^{2+}, Mn^{2+}. According to the analysis of crystal structure and emission spectra, we can conclude that the emission band of Mn^{2+} from shorter to longer wavelength sides are attribute to the Mn^{2+} ions at Mg(III), Mg(II) and Mg(I) sites, respectively. The energy transfer between the Eu^{2+} and Mn^{2+} ions is of a resonant type via a dipole–quadrupole mechanism. The stronger crystal field and the energy transfer between the Mn^{2+} ions are responsible for the emission redshift with increasing Mn^{2+} concentration and operating temp. The emission colors of the obtained phosphors could be tuned from blue (0.1479, 0.0663) to pink (0.2683, 0.1496) by controlling the doping of Mn^{2+}. These results demonstrate that the $KMg_4(PO_4)_3$: Eu^{2+}, Mn^{2+} phosphor may have potential application for white light-emitting diodes and plantlets cultured.

Acknowledgements

We thank Y. J. Wang for help with the quantum efficiency and luminous efficiency measurements, Chongqing University of Posts and Telecommunications, China. We also gratefully thank the financial support from the Program for New Century Excellent Talents in University of Ministry of Education of China (Grant No. CET-12-0951), the Fundamental Research Funds for the Central Universities (Grant No. 2652015020) and the National Natural Science Foundation of China (Grant No. 51472223).

Notes and references

Beijing Key Laboratory of Materials Utilization of Nonmetallic Minerals and Solid Wastes, National Laboratory of Mineral Materials, School of Materials Science and Technology, China University of Geosciences, Beijing, 100083, China. E-mail: liuyang@cugb.edu.cn; Tel./Fax: +86-10-82322186

1 H. Zhu, C. C. Lin, W. Luo, R. S. Shu, Z. G. Liu, Y. S. Liu, J. T. Kong, E. Ma, Y. G. Cao, R. S. Liu and X. Y. Chen, *Nat. Commun.,* 2014, **5,** 4312.

2 V. Bachmann, C. Ronda, O. Oeckler, W. Schnick and A. Meijerink, *Chem. Mater*., 2008, **21,** 316-325.

3 R. E. Nlankenship, D. M. Tiede, J. Barber, G. W. Brudvig, G. Fleming and M. Ghirardi, *Science.,* 2011, **332,** 805-809.

4 R. Zhang, H. Lin, Y. L. Yu, D. Q. Chen, J. Xu and Y. S. Wang, *Laser Photonics Rev.,* 2014, **8,** 158-164.

5 D. Q. Chen, *J. Eur. Ceram. Soc.,* 2014, **34,** 4069-4075.

6 L. Wondraczek, M. Batentschuk, M. A. Schmidt, R. Borchardt, S. Scheiner, B. Seemann, P. Schweizer and C. J. Brabec, *Nat. Commun.,* 2013, **4,** 2047-1-6.

7 D. T. Nhut, T. Takamura, H. Watanabe, K. Okamoto and M. Tanaka, *Plant. Cell. Tiss. Org*., 2003, **73,** 43-52.

8 G. Tamulaitis, P. Duchovskis, Z. Bliznikas, K. Breive, R. Ulinskaite, A. Brazaityte and *A.* Žukauskas, *J. Phys. D. Appl. Phys*., 2005, **38,** 3182-3187.

9 M. E. Hoenecke, R. J. Bula and T. W. Tibbitts, *HortScience.,* 1992, **27,** 427-430.
10 C. G. Lee and B. O. Palsson, *Biotech. Bioeng.,* 1994, **44,** 1161-1167.
11 D. J. Tennessen, E. L. Singsaas and T. D. Sharkey, *Photo. Res.,* 1994, **39,** 85-92.
12 B. C. Tripathy and C. S. Brown, *Plant Physiol.,* 1995, **107,** 407-411.
13 C. Robin, M. J. M. Hay and P. C. D. Newton, *Oecologia.,* 1994, **100,** 236-242.
14 C. Robin, M. J. M. Hay, P. C. D. Newton and Greer, *Ann. Bot.,* 1994, **72,** 119-123.
15 A. Kurilčik, R. Miklušytė-Čanova, S. Dapkūnienė, S. Žilinskaitė, G. Kurilčik, G. Tamulaitis and A. Žukauskas, *Cent. Eur. J. Biol.*, 2008, **3,** 161-167.
16 L. Shi, Y. Huang and H. J. Seo, *J. Phys. Chem. A.,* 2010, **114,** 6927-6934.
17 M. Y. Peng, X. Yin, P. A. Tanner, C. Liang, P. Li, Q. Zhang and J. R. Qiu, *J. Am. Ceram. Soc*., 2013, **96,** 2870-2876.
18 J. Chen, Y. G. Liu, M. H. Fang and Z. H. Huang, *Inorg. Chem.,* 2014, **53,** 11396-11403.
19 C. C. Lin and R. S. Liu, *J. Phys. Chem. Lett.,* 2011, **2,** 1268-1277.
20 M. M. Shang, C. X. Li and J. Lin, *Chem. Soc. Rev.,* 2014, **43,** 1372-1386.
21 W. R. Liu, C. H. Huang, C. W. Yeh, J. C. Tsai, Y. C. Chiu, Y. T. Yeh and R. S. Liu, *Inorg. Chem.,* 2012, **51,** 9636-9641.
22 P. E. Tomaszewski, M. Maczka, A. Majchrowski, A. Waskowska and J. Hanuza, *Solid. State. Sci.,* 2005, **7,** 1201-1208.
23 X. F. Lan, Q. Q. Wei, Y. Y. Chen and W. J. Tang, *Opt. Mater.,* 2012, **34,** 1330-1332.
24 C. M. Liu, D. J. Hou, J. Yan, L. Zhou, X. J. Kuang, H. B. Liang, Y. Huang, B. B. Zhang and Y. Tao, *J Phys Chem C.*, 2014, **118,** 3220-3229.
25 A. M. Pires and M. R.Davolos, *Chem. Mater*., 2001, **13,** 21-27.
26 H. K. Liu, L. B. Liao and Z. G. Xia, *RSC Adv.,* 2014, **4,** 7288-7295.
27 P. I. Paulose, G. Jose, V. Thomas, N. V. Unnikrishnan and M. K. R. Warrier, *J. Phys. Chem. Solids*., 2003, **64,** 841-846.
28 D. L. Geng, G. G. Li, M. M. Shang, D. M. Yang, Y. Zhang, Z. Y. Cheng and J. Lin, *J. Mater. Chem.,* 2012, **22,** 14262-14271.
29 S. Sugano, Y. Tanabe and H. Kamimura, *Multiplets of Transition-Metal Ions in Crystals*, Academic: New York, 1970.
30 J. Wang, Z.Y. Zhang, M. Zhang, Q.H. Zhang, Q. Su and J. K. Tang, *J. Alloys. Compd.,* 2009, **488,** 582-585.
31 W. J. Yang, L. Luo, T. M. Chen and N. S. Wang, *Chem. Mater.,* 2005, **17,** 3883-3888.
32 H. K. Liu, Y. Luo, Z. Y. Mao, L. B. Liao and Z. G. Xia, *J. Mater. Chem. C*., 2014, **2,** 1619-1627.
33 D. Q. Chen, W. D. Xiang, X. J. Liang, J. S. Zhong, H. Yu, M. Y. Ding, H. W. Lu and Z. G. Ji, *J. Eur. Ceram. Soc.,* 2015, **35,** 859-869.
34 G. Blasse and B. C. Grabmarier, *Luminescent Materials*; Springer-Verlag: Berlin, Germany, 1994; p 96.
35 J. Chen, Y. G. Liu, H. K. Liu, D. X. Yang, H. Ding, M. H. Fang and Z.H. Huang, *Rsc Adv.,* 2014, **4,** 18234-18239.
36 Z. G. Xia, J. Zhou and Z. Y. Mao, *J. Mater. Chem. C*., 2013, **1,** 5917-5924.
37 D. L. Dexter and J. H. Schulman, *J. Chem. Phys.,* 1954, **22,** 1063-1070.
38 C. Guo, H. Jing and T. Li, *RSC Adv.*, 2012, **2,** 2119-2122.
39 C. H. Huang and T. M. Chen, *J. Phys. Chem. C.,* 2011, **115,** 2349-2355.
40 G. Blasse, *Philips Res. Rep.,* 1969, **24,** 131-144.
41 Y. C. Chiu, W. R. Liu, C. K. Chang, C. C. Liao, Y. T. Yeh, S. M. Jang and T. M. Chen, *J. Mater. Chem.,* 2010, **20,** 1755-1758.
42 D. L. Dexter, *J. Chem. Phys.,* 1953, **21,** 836-850.
43 E. Song, W. Zhao, G. Zhou, X. Dou, C. Yi and M. Zhou, *J. Rare. Earth.,* 2011, **29,** 440-443.
44 V. B. Mikhailikm, H. Kraus, D. Wahl, M. Itoh, M. Koike, I. K. Bailiff, *Phys. Rev.,* 2004, **69B,** 20510-205110-9.
45 Y. P. Varshni *Phys.,* 1967, **34,** 149-154.
46 J. S. Kim, Y. H. Park, S. M. J. Kim, C. Choi and H. L. Park, *Solid State Commun*., 2005, **133,** 445-448.
47 K. H. Kwon, W. B. Im, H. S. Jang, H. S. Yoo and D. Y. Jeon, *Inorg. Chem.,* 2009, **48,** 11525-11532.

Emission Red Shift and Energy Transfer Behavior of Color-tunable $KMg_4(PO_4)_3$:Eu^{2+}, Mn^{2+} Phosphors

Jian chen, Yangai Liu, Lefu Mei, Ziyao Wang, Minghao Fang and Zhaohui Huang*

Beijing Key Laboratory of Materials Utilization of Nonmetallic Minerals and Solid Wastes, National Laboratory of Mineral Materials, School of Materials Science and Technology, China University of Geosciences, Beijing, 100083

A series of Eu^{2+} and Mn^{2+} -co activated $KMg_4(PO_4)_3$ phosphor was prepared by the conventional high temperature solid-state reaction. Their luminescence properties and energy transfer between Eu^{2+} and Mn^{2+} were investigated, respectively. The wavelength position of emission red shift, full wavelength at half-maximum (FWHM), temperature-dependent emission spectra, and color coordinates were investigated and the related mechanisms were discussed in detail.

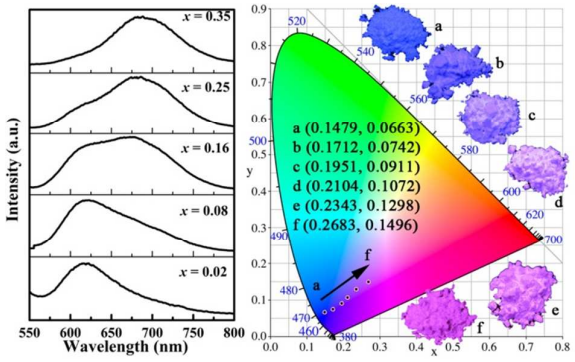

*Corresponding author: Tel./Fax: +86-10-82322186

E-mail addresses: liuyang@cugb.edu.cn (Y.G. Liu)